nature photonics

ARTICLES

https://doi.org/10.1038/s41566-020-0604-2

Deep-learning-enabled self-adaptive microwave cloak without human intervention

Chao Qian[1,2], Bin Zheng[1,2], Yichen Shen[3,4], Li Jing[3], Erping Li[1,2], Lian Shen[1,2] and Hongsheng Chen[1,2]✉

Becoming invisible at will has fascinated humanity for centuries and in the past decade it has attracted a great deal of attention owing to the advent of metamaterials. However, state-of-the-art invisibility cloaks typically work in a deterministic system or in conjunction with outside help to achieve active cloaking. Here, we propose the concept of an intelligent (that is, self-adaptive) cloak driven by deep learning and present a metasurface cloak as an example implementation. In the experiment, the metasurface cloak exhibits a millisecond response time to an ever-changing incident wave and the surrounding environment, without any human intervention. Our work brings the available cloaking strategies closer to a wide range of real-time, in situ applications, such as moving stealth vehicles. The approach opens the way to facilitating other intelligent metadevices in the microwave regime and across the wider electromagnetic spectrum and, more generally, enables automatic solutions of electromagnetic inverse design problems.

Rendering an object invisible with an invisibility cloak is a long-standing dream for humanity, with potential in many interesting applications. For example, it would be very exciting to drive a stealth vehicle through different environments—hills, plains, deserts and so on—without being detected. Such a scenario was inconceivable until the proposal of transformation optics[1] and metamaterials[2]. A transformation optics-based cloak produces invisibility through precise design of its constitutive parameters so as to guide the flow of light around a hidden object, but it is a major challenge to experimentally achieve bulky material compositions with both anisotropy and inhomogeneity[3–6]. Other invisibility methodologies, such as scattering cancellation[7,8] and gradient metasurface coating[9–11], have also been proposed in the form of electromagnetic (EM)[1–11], sound[12] and elastic waves[13] or heat flows[14], depending on the application scenario.

In reaction to an external stimulus or non-stationary environment, an ideal invisibility cloak should rapidly and automatically adjust its internal structure—its active components—to remain invisible at all times, as if the cloak were endowed with a chameleon's ability. This highly desirable but not easily attainable property—intelligent or self adaptability—must be developed so as to be applicable to a wide range of real-time applications involving moving objects and in situ environments. For this, it is essential to be able to interpret the intricate and non-intuitive relationships among the cloaking structure, incoming light and surrounding environment and then impart this knowledge/experience to the cloak. However, the strategies currently available to process light–matter interactions typically involve case-by-case full-wave simulations and bottom-up design, which limits the application scope in several ways. First, because full-wave simulations involve iterative and lengthy calculations of Maxwell's equations, they are inherently time-consuming procedures[15,16]; this inevitably degrades the efficiency of a cloak and limits its ability to react on short timescales. Second, in the pursuit of a desired nanostructure, there will be many failed attempts; these are usually discarded, leading to a waste of resources[17]. Finally, the used strategy should be able to react rapidly to gradual changes in a scenario (for example, in the optical environment); such changes in the cloak's response are non-trivial because of the strong nonlinear and elusive nature of light–matter interactions[18]. Programmable and reconfigurable metamaterials and so-called adaptive EM devices have been extensively studied and underpin the performance of some established technologies[19–21], but they also need to work in tandem with outside input (dependent, non-autonomous) and in a trial-and-error mode in order to meet customer-specific requirements, strongly hindering real-time applications (Supplementary Note 11). Given all these factors, an effective approach to avoid time-consuming repeated manual labour and develop self-adaptability in invisibility cloaks is highly sought after, but challenging to achieve.

In this Article, we propose the concept of an intelligent invisibility cloak driven by deep learning and build an example of such a cloak with a tunable metasurface (Fig. 1). The reflection property of each element inside the metasurface can be independently tuned by feeding different direct-current (d.c.) bias voltages across a loaded varactor diode[19] at microwave frequencies. Embedded with a pretrained artificial neural network (ANN), a fundamental building block of deep learning, the metasurface cloak can respond rapidly, on a millisecond timescale, to the ever-changing incident wave and surrounding background, without any human intervention. All the bias voltages are automatically calculated and instantly supplied to the cloak. We use a finite-difference time-domain (FDTD) program[22,23] with the pretrained ANN to imitate a real-world scene and then benchmark the performance via a proof-of-concept experiment. This verifies that the metasurface cloak exhibits effective and robust self-adaptability in response to a random incident wave and background. Our work brings the available cloaking strategies closer to practical scenarios involving changing backgrounds, moving objects, multi-static detection and beyond, and it can be

[1]State Key Laboratory of Modern Optical Instrumentation, Interdisciplinary Center for Quantum Information, College of Information Science and Electronic Engineering, Zhejiang University, Hangzhou, China. [2]ZJU-Hangzhou Global Science and Technology Innovation Center, Key Laboratory of Advanced Micro/Nano Electronic Devices & Smart Systems of Zhejiang, ZJU-UIUC Institute, Zhejiang University, Hangzhou, China. [3]Department of Physics, Massachusetts Institute of Technology, Cambridge, MA, USA. [4]Lightelligence Inc., Boston, MA, USA. ✉e-mail: hansomchen@zju.edu.cn

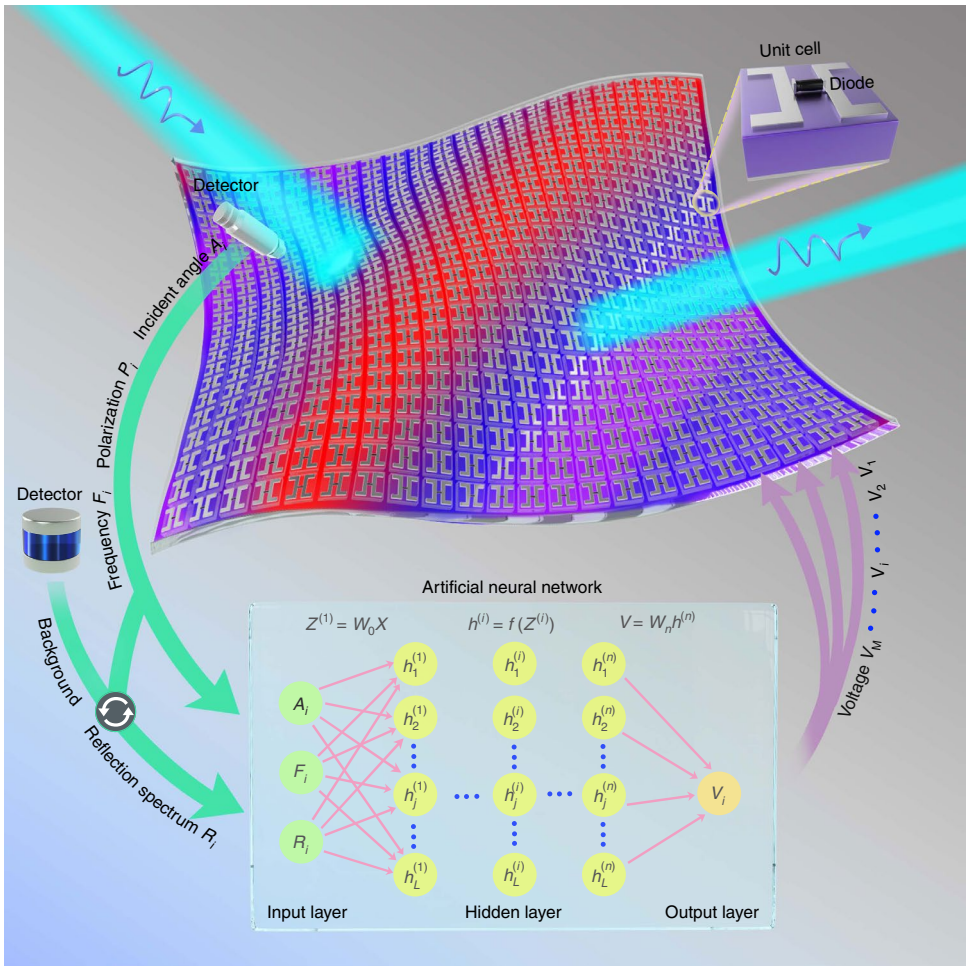

Fig. 1 | Schematic of a deep-learning-enabled self-adaptive metasurface cloak. The metasurface cloak is composed of an ultrathin layer of active meta-atoms, each incorporating a varactor diode that is independently controlled by a d.c. bias voltage (upper right corner). In response to a detected incident wave and the surrounding background, all bias voltages are automatically calculated by the pretrained ANN and instantly supplied by a power supply platform. Note that the detected background information is converted to the required reflection spectrum for each meta-atom based on the wave reconstruction method[9] and then fed to the pretrained ANN as an input. See Supplementary Note 7 for a description of the operating principle.

readily scaled up to higher frequencies (Supplementary Note 12). Moreover, the proposed concept will lead to a new genus of intelligent metadevices and the manipulation of EM waves in an unsupervised fashion[24].

Architecture of the intelligent invisibility cloak

The architecture of the intelligent metasurface cloak is outlined in Fig. 1. It contains five main parts: the tunable reconfigurable metasurface inclusion, two detectors (for the incident wave and the surrounding background), the pretrained ANN and a power supply platform. The ultrathin metasurface inclusion consists of many active unit cells/meta-atoms, each providing a different local reflection spectrum and thus producing a scattered wave similar to that generated by the bare surrounding without a hidden object. The local reflection spectrum, containing both amplitude and phase, is derived from the surrounding background, cloak location and incident wave via the wave reconstruction method[9] (Supplementary Note 7). A varactor diode is incorporated into each meta-atom (upper right corner, Fig. 1), and its reflection spectrum can be dynamically altered by feeding different d.c. bias voltages (output of the architecture) across it at microwave frequencies[19,20]. As well as this active approach, electrical gating, mechanical actuation, phase-change materials and magneto-optic control can also be employed at their natural frequencies, ranging from microwave to optical and even visible frequencies[25]. Metasurface cloaking (and other metamaterial cloaks) relies largely on precise local phase manipulation—the electric or magnetic response—of resonant elements in order to reconstruct the scattered light[10]. For a particular type of structure or state, such a cloak thus normally works over a narrow bandwidth, with a limited incident angle and with a stationary background[11]. When the incident wave or background changes, such a metasurface cloak may become inefficient and even disabled. Here, the factors affecting the cloak are detected in real time and transformed into the requisite local reflection spectrum as one input to the ANN (Supplementary Fig. 12). Meanwhile, the detected incident wave is set as the other input due to the strong frequency dispersion and non-local effect of the metasurface[19,26]; this incident wave is characterized by its incident angle, frequency and polarization.

By using deep learning we aim to exploit and generalize the intricate relationship {incident wave and reflection spectrum} → {bias voltage} for an individual meta-atom (Supplementary Fig. 12). The pretrained ANN is used in parallel with many such meta-atoms inside a metasurface cloak that is covering a large object (Supplementary Fig. 13); in this way we apply the ANN model to a complex application. Recently, deep learning has been used to significantly improve state-of-the-art mainstream applications such as image/speech recognition, translation and healthcare[27,28], but it has

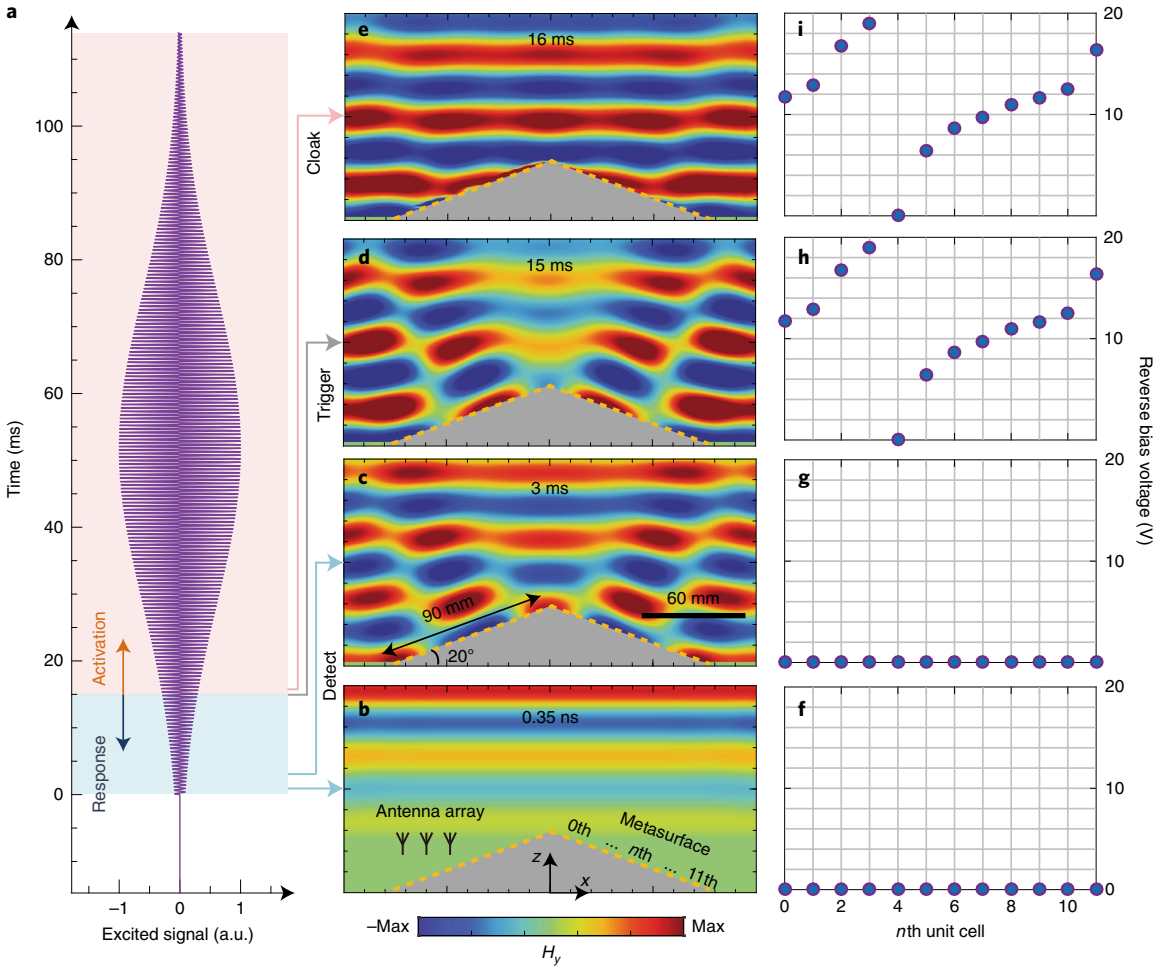

Fig. 2 | Transient response of the self-adaptive cloak in FDTD simulations. a, A Gaussian pulse emitted from $z = 120$ mm impinges on the triangular PEC bump covered by the metasurface; its waveform satisfies $g(t) = \cos(2\pi \times f_c \times (t - t_0))e^{-((t-t_0)/\tau)^2}$ with centre frequency $f_c = 8$ GHz, $\tau = 33$ ns and $t_0 = 52$ ns. **b**–**e**, Time evolution (0.35 ns (**b**), 3 ns (**c**), 15 ns (**d**) and 16 ns (**e**)) of magnetic field H_y within the observation region (120 mm × 240 mm). During this process, the incident information is detected by an antenna array and then fed into the pretrained ANN, together with a hypothetically known background. At $t = 15$ ns (**d**), the metasurface cloak is triggered, and subsequently renders the bump invisible. **f**–**i**, Distributions of the reverse bias voltages corresponding to **b**–**e**, respectively. Owing to the geometrical symmetry, the bias voltages along the two bevel edges are identical under normal incidence.

also penetrated into other disciplines, such as materials science and quantum mechanics[29,30]. As shown in Fig. 1, an ANN normally consists of a set of input artificial neurons that are interconnected to a number of hidden layers and one output layer. Information propagates forward via a linear operation such as matrix multiplication, followed by a nonlinear activation function. Before putting an ANN into use, the synaptic strengths between each layer need to be adequately trained via a back-propagation algorithm such as a gradient descent or adaptive optimizer.

Transient response of the intelligent cloak using FDTD simulations

For conceptual clarity, we consider a two-dimensional (2D) metasurface carpet cloak under transverse-magnetic (TM, or *p*-polarized) polarized illumination. The metasurface cloak is carefully designed to conceal a perfect electrical conductor (PEC) bump or other object in free space. For each unit cell, a reverse d.c. bias voltage ranging from 0 to 20 V is provided to control the capacitance of the varactor diode and tune the reflection spectrum (the reflection phase covers almost −180° to 180° within the working range). Details about the unit cell and its equivalent circuit model are provided in Supplementary Notes 1 and 2.

To show how the intelligent cloak works, an FDTD algorithm inserted with the pretrained ANN is used to observe the transient response of the intelligent cloak (see Supplementary Note 3 for the simulation set-up). Combined with an antenna array for incident wave detection (see Methods) and a hypothetically known surrounding environment, a full set of the simulation program (that is, the EM numerical algorithm for the cloak, the pretrained ANN and an algorithm for detecting incident waves) is built to imitate a real-world scene. In the simulation, a TM plane wave with a random cosine-modulated Gaussian waveform is incident on the cloak; the waveform and physical images at different times are plotted in Fig. 2. In the initial state, all bias voltages are set to zero. As time passes, the incident wave interacts with the bump, strongly distorting the scattered waves, as shown in Fig. 2c. After ~15 ns (the practical response time), the detector receives the incident wave information and feeds it to the pretrained ANN. The metasurface cloak is triggered (Fig. 2d) and renders the bump invisible (Fig. 2e). This example demonstrates the operation of the intelligent cloak in the time domain.

Experiment and ANN training

For the experiment we chose an F4B material with a dielectric constant of 3.5 and a loss tangent of 0.003 as the substrate. A photograph

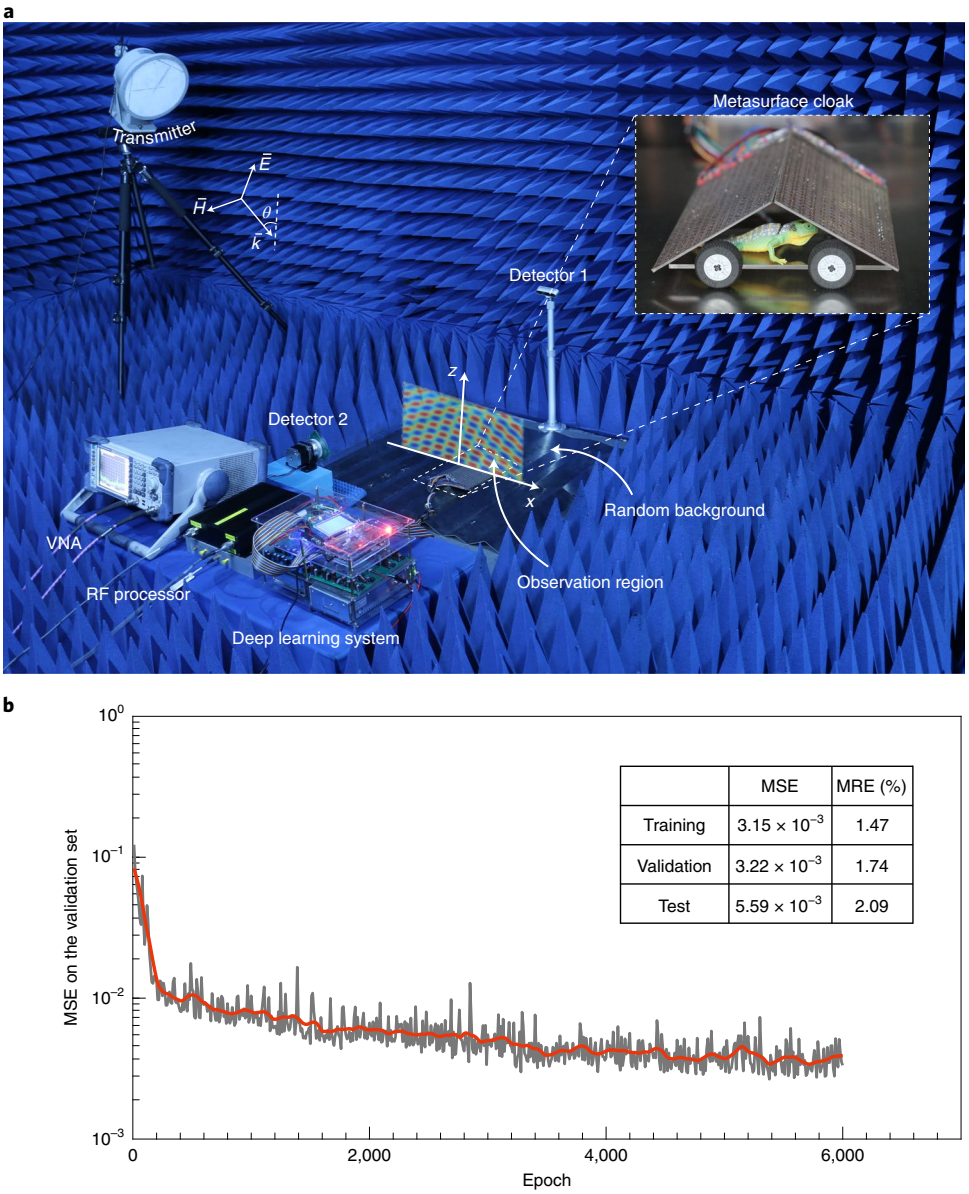

Fig. 3 | Experimental set-up and ANN training results. a, A TM-polarized Gaussian beam from a high-directivity lens antenna is incident on the scatterer with incident angle θ. The observation region (200 mm × 400 mm) is at a height of 60 mm above the ground, and the cloak geometry is consistent with that in Fig. 2. The surrounding background and incident wave are detected in real time by detectors 1 and 2, respectively (see Supplementary Note 5 for details), fed into the deep learning system, and all bias voltages are instantly calculated and supplied to the metasurface cloak. This process takes ~15 ms. Inset: photograph of the fabricated prototype. VNA, vector network analyser; RF, radio frequency. **b**, The mean square error (MSE) of the validation set over the epoch, shown as a grey curve. The orange curve shows the smoothed MSE. The inset table lists the final MSE and mean relative error (MRE) for the three listed sets.

of the fabricated prototype (made using conventional printed circuit board technology) is provided in Fig. 3a. The dimensions of the metasurface inclusion are 180 × 210 × 2 mm^3 (24 × 28 unit cells); this is divided into two identical pieces. Every column (28 unit cells) along the y direction shares the same bias voltage, with varactor diodes welded between the metallic split I-shaped islands on the dielectric substrate. Instead of the simulated results, we experimentally measured the reflection spectrum for the flat metasurface under different incident waves and bias voltages[19] as training samples (Supplementary Note 4). The suppressed reflection amplitude of the meta-atom in Supplementary Fig. 4 is mainly caused by the intrinsic resistance of the varactor diode, which can be further improved by using a microwave gain medium[31].

We trained the ANN with the relation {incident wave and reflection spectrum} → {bias voltage} for the meta-atoms using ~10,000 measured samples (Supplementary Note 8), which were split into training, validation and test sets (80%, 10% and 10%, respectively). The inputs were normalized, shuffled and then fed into the network, as this treatment can accelerate convergence of the algorithm. Mean square error (MSE) was used to represent a loss function between the normalized and desired output and the loss of the training set was used to generate gradients (pure learning). The hyperparameters (for example, number of hidden layers, neurons and learning rates) were set according to the performance on the validation set[18]; ultimately, a fully connected network with five hidden layers and 60 neurons per layer was selected (Supplementary Note 8).

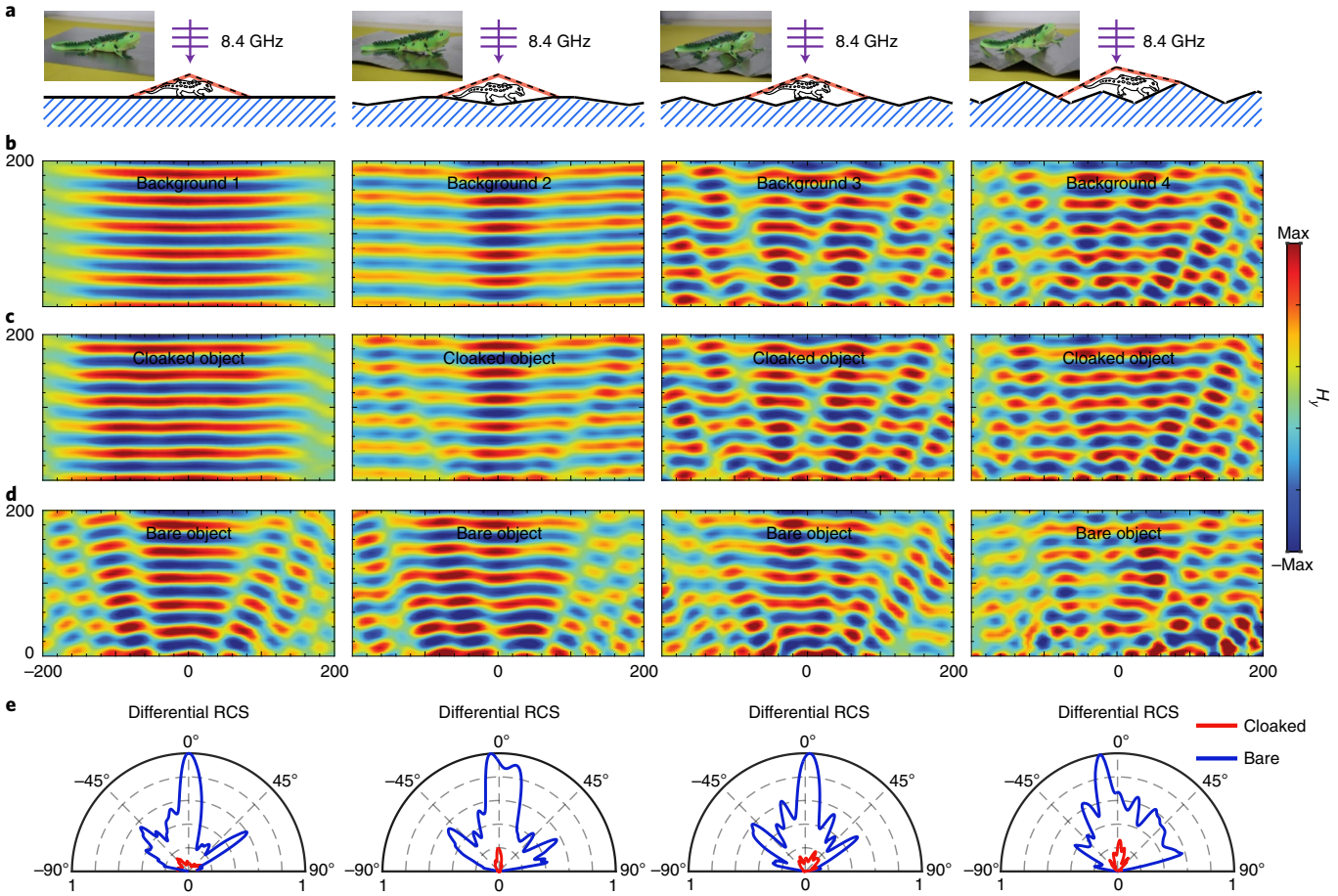

Fig. 4 | Demonstration of the self-adaptive cloak response to random backgrounds for normal wave incidence at 8.4 GHz. a, Schematic of the four backgrounds 1–4. The grey dashed line attached to the red line delineates the metasurface cloak. The object used for demonstration of the cloaking capability is a chameleon-shaped plastic model and can be changed to any arbitrary object of a similar size. **b**–**d**, Near-field magnetic field H_y distributions of the background (**b**), cloaked object (**c**) and bare object (**d**), respectively (in mm). **e**, Far-field differential RCS of the cloaked and bare objects for the four cases. Measurement details are provided in Supplementary Note 6.

For illustrative purposes, the mean relative error (MRE) is defined as the mean percent off per point on the bias voltages (by finding the error between the output and the desired value, then normalizing by the magnitude). As listed in the inset table in Fig. 3b, the MREs of the three sets are all less than 2.1% and match each other closely, suggesting that the trained ANN is smooth and almost without overfitting. We can thus safely conclude that the pretrained ANN is credible and applicable in this scenario.

Figure 3a presents the full experimental system used to verify the performance of the intelligent cloak corresponding to the layout in Fig. 1. The pretrained ANN and power module are integrated together (labelled 'deep learning system'). The incident wave (including frequency and incident angle) and the surrounding environment are detected in real time by a high-directivity Vivaldi antenna and depth camera, respectively (see Supplementary Note 5 for the design details). We first derive the required reflection spectra for all meta-atoms (the conversion time is so short that it can be ignored) and then input them, in parallel, into the pretrained ANN (Supplementary Fig. 13). The response time, including detection (the part that takes longer) and the ANN computing and instruction time, is ~15 ms. This can be reduced further by using a phase-array radar, for example, assisted by a direction-of-arrival algorithm such as MUSIC or ESPRIT[32,33].

In our first experiment, we investigated scenarios with a TM-polarized Gaussian beam from a lens antenna impinging normally on a scatterer on four random backgrounds/landforms (blue hashed areas) (Fig. 4a). The near-field magnetic field distributions over the landform (Fig. 4b, labelled 'background'), the cloaked object (Fig. 4c) and the bare object (Fig. 4d) were scanned (Supplementary Fig. 9a). The object used to demonstrate the cloaking capability (here a chameleon-shaped plastic model) can be changed to any arbitrary object of a similar size. The field patterns generated by the cloaked object are analogous to those generated by the surroundings, in stark contrast to those for the bare object, where the scattered waves are drastically distorted. The slight discrepancies in the rightmost panels in Fig. 4b,c might arise because the detector we used is not accurate enough to characterize the complex surrounding landform; this could be improved by using more advanced detectors such as laser radar. To quantitatively demonstrate the cloaking performance, the differential radar cross-section (RCS) was defined as $\sigma_{\mathrm{cloaked/bare}} = 2\pi\rho\left|H_y^{\mathrm{c/b}} - H_y^{\mathrm{g}}\right|^2$, where H_y^{c}, H_y^{b} and H_y^{g} are the magnetic field in the cloaked object, bare object and background cases, respectively[11], and ρ is set to 1.3 m for the far-field approximation[34] (Supplementary Fig. 9b). Figure 4e shows that the differential RCS of the cloaked object is highly suppressed for all four landforms, with a reduction in total RCS of more than 85%. We benchmarked the intelligent cloak in a second experiment (Fig. 5), in which the incident angle, frequency and landform varied simultaneously. The cloaked object is shown to successfully offset the external illumination

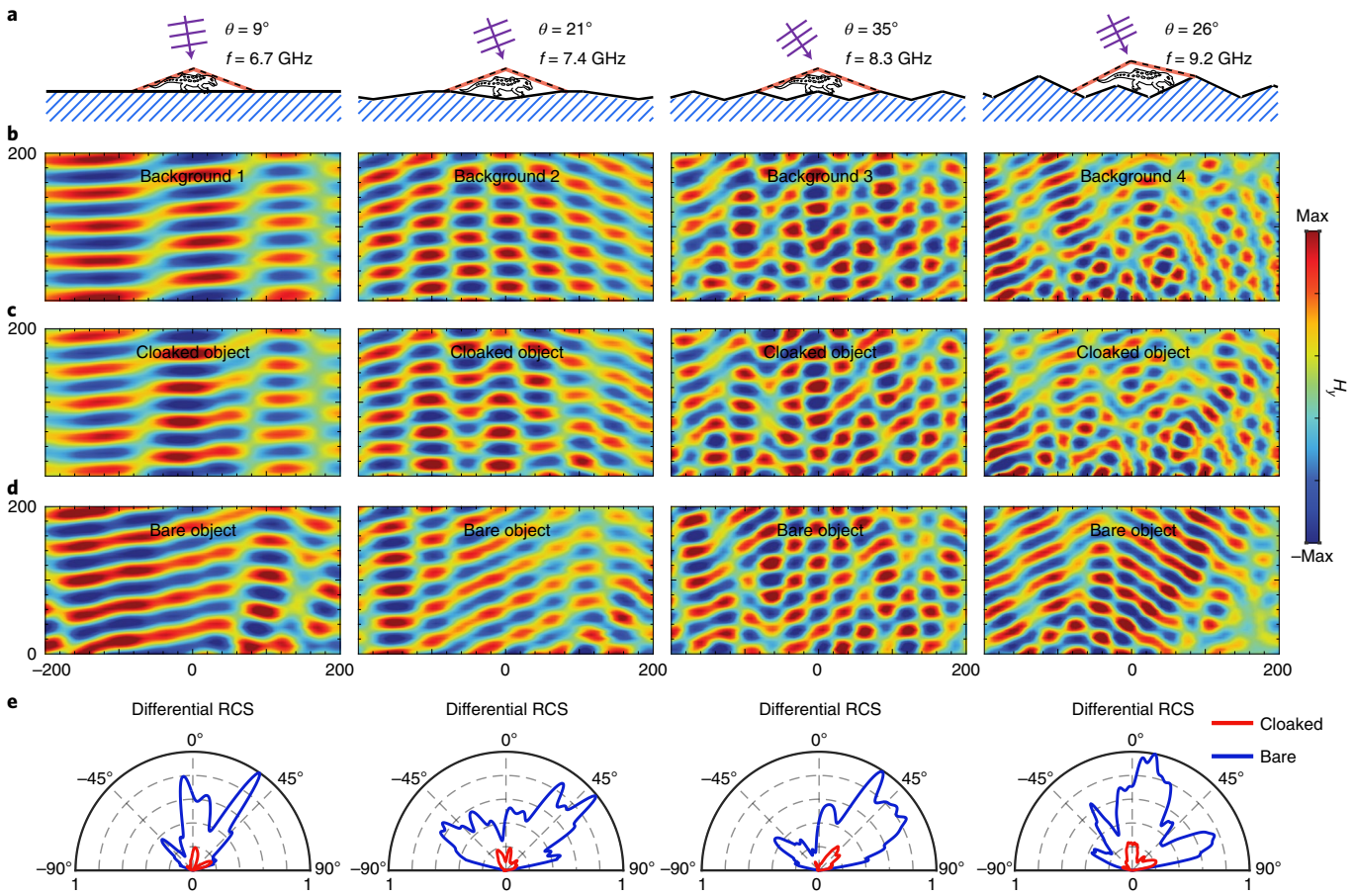

Fig. 5 | Demonstration of the self-adaptive cloak response to random and simultaneous changes in the incident wave and background. a, Schematic of the background and the incident wave. **b**–**d**, Near-field magnetic field H_y distributions of the background (**b**), cloaked object (**c**) and bare object (**d**), respectively (in mm). **e**, Far-field differential RCS of the cloaked and bare object for the four cases.

and blends itself into the surrounding environment. In each experiment, the reaction is completed on a millisecond timescale, whereas a chameleon needs ~6 s. These multi-variable experiments strongly validate the robustness of our intelligent cloak. Supplementary Note 10 shows more results, and Supplementary Video 1 demonstrates the performance of a cloaked vehicle passing through a random landform, compared with the uncloaked case.

Discussion

In practice, backgrounds are changing constantly, which is a great challenge to generalize with limited samples, especially for the applications of image recognition and classification. That said, for the metasurface cloak, the background information can be epitomized in a series of local reflection spectra provided by the meta-atoms (Supplementary Note 7). The local reflection spectra are generalized and all cases are exemplified in our collected dataset. If we treat the background or the induced global reflection spectra as the input of the ANN, the data collection itself will be very cumbersome and a huge burden, as numerous samples would be required. This is why we construct the ANN to map {incident wave and reflection spectrum} → {bias voltage} for individual unit cells and apply this to each unit cell inside the metasurface cloak (Supplementary Fig. 13). In each experiment, the collective action of all unit cells (672 in our case), rather than an individual cell or some unit cells, leads to the cloaking effect. The 672 inputs may simultaneously contain data from the training, validation and test sets. This is normal in deep learning; for example, in a translation task, there may be parts of phrases in the test set that exist in the training set. It is important to note that, although all the inputs are from the test set, like the experiment in the leftmost panel of Fig. 5c, the cloaking effects are also quite satisfactory.

The working range of the metasurface cloak with bandwidth of 6.7–9.2 GHz is inherently restricted by the capacitance range of the varactor diode and the resonant structure, rather than by the constraints of the intelligent system. Both the simulated and experimental results support this fact. An active cloaking strategy[35] that uses an array of elementary sources to offset the scattered fields caused by the hidden object may take this a step further, potentially realizing an intelligent cloak over a broad bandwidth. Meanwhile, the concept of the intelligent cloak can be scalable to higher frequencies. At optical frequencies, we can construct spatially phase-modulated masks with gate-tunable conducting oxide metasurfaces such as indium tin oxide[36] or phase-changing materials such as germanium antimony tellurium[37] and vanadium dioxide[38] (see Supplementary Note 12 for the actual strategies). Furthermore, the single polarization limitation of this work can be overcome by hybridizing multiple diodes along non-parallel or orthogonal orientations[39], together with a more sophisticated network configuration.

In the design of nanostructures, conventional full-wave simulations rely heavily on iterative and lengthy calculations of Maxwell's equations, guided by an optical expert, until a locally optimized solution is attained. An alternative approach, an equivalent circuit model[40], is fast, but is used empirically only for rough analysis and for simple structures and cases; it is thus infeasible for applications that require high precision (Supplementary Note 2), such as the present metasurface cloak. Deep learning lifts these limitations by automatically discovering powerful nonlinear feature combinations

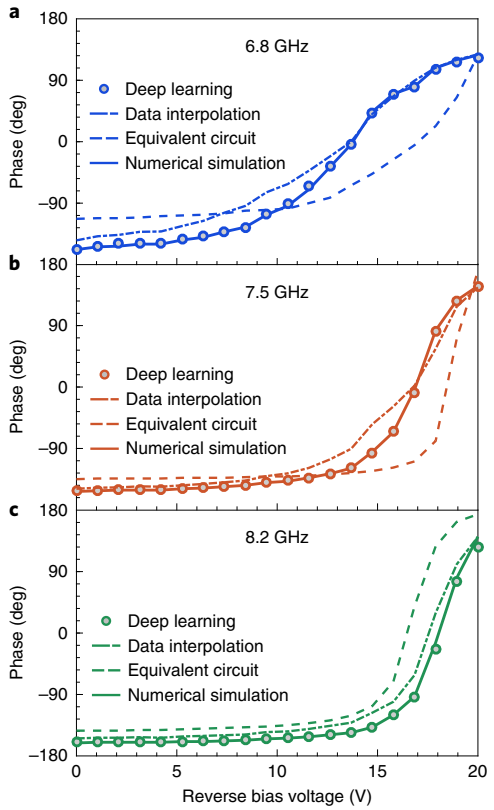

Fig. 6 | Reflection spectrum of the metasurface obtained by different methods. a–**c**, Reflection phase of the metasurface versus applied bias voltage under normal incidence at three different frequencies: 6.8 GHz (**a**), 7.5;GHz (**b**) and 8.2 GHz (**c**). The ANN predictions (completed on a millisecond timescale) match well the real spectrum obtained by simulation (obtained on the second or even minute timescale). In contrast, the phase curves plotted with the linear data interpolation and the equivalent circuit model are far from reality, although the millisecond runtime is promising. More discussions on data interpolation and the equivalent circuit model are provided in Supplementary Notes 2 and 9.

with unrivalled accuracy and efficiency, as shown in Fig. 6 (plotted by flipping the pretrained ANN backwards; Supplementary Note 9). We also note that the superiorities of deep learning will be significantly pronounced in high-throughput, real-time, in situ and complex scenarios such as practical 3D cloak and multi-static detection.

Establishing data for the ANN may need some time, but there are at least two reasons why the method is still useful. First, the hardware is inexpensive and, to save time, data generation can be performed easily in parallel across machines. In our work, the 10,000 samples (on average, sampling only 10 times over frequencies 6–10 GHz, 20 times over incident angles −90°–90° and 50 times over reflection phase 0–2π) are easily accessed with little effort, yielding the pretrained ANN with high fidelity. Supplementary Note 8 explains that the 10,000 samples are sufficient in our work and the MRE is consistently low (3.9%), even though the trained samples are reduced by half (Supplementary Fig. 14). Second, as indicated in Fig. 6, the staggering enhancement of both accuracy and efficiency is well worth the tradeoff. Beyond this, once the ANN is pretrained, it can be applied to other functionalities, such as optimizing structures and flipping it backwards to predict a user-favoured EM response.

Conclusion

We have proposed the concept of an intelligent cloak driven by deep learning and have implemented a metasurface cloak as an example. Embedded with a pretrained ANN, the metasurface cloak exhibits effective and robust self-adaptability in response to an ever-changing incident wave and background, without human intervention. The single feed-forward computation in the ANN saves a significant amount of time compared with the repeated iterative calculations required in an adaptive antenna[41] and adaptive optics[42] (Supplementary Note 11). This concept has been verified by FDTD simulations and a proof-of-concept microwave experiment, which moves cloaking research into its next stage—intelligent cloaks. The proposed concept not only paves the pathway towards radically new metadevices, but also other big data areas, such as streamlining the on-demand design of nanostructures[15,16,18], solving the EM inverse problem[43] and capturing latent physical knowledge[44]. In turn, classical electromagnetics and optics will foster the development of deep learning. For example, compared with conventional microelectronic implementations, optical ANNs using nanophotonic circuits[45] and metasurfaces[46] could offer an enhancement of computing speed and power efficiency. We are already witnessing the interplay between these two seemingly unrelated disciplines and anticipate more exciting works.

Online content

Any methods, additional references, Nature Research reporting summaries, source data, extended data, supplementary information, acknowledgements, peer review information; details of author contributions and competing interests; and statements of data and code availability are available at https://doi.org/10.1038/s41566-020-0604-2.

Received: 17 April 2019; Accepted: 12 February 2020;
Published online: 23 March 2020

References

1. Pendry, J. B., Schurig, D. & Smith, D. R. Controlling electromagnetic fields. *Science* **312**, 1780–1782 (2006).
2. Engheta, N. & Ziolkowski, R. W. *Metamaterials*: *Physics and Engineering Explorations* (Wiley, 2006).
3. Schurig, D. et al. Metamaterial electromagnetic cloak at microwave frequencies. *Science* **314**, 977–980 (2006).
4. Cai, W., Chettiar, U. K., Kildishev, A. V. & Shalaev, V. M. Optical cloaking with metamaterials. *Nat. Photon.* **1**, 224–227 (2007).
5. Landy, N. & Smith, D. R. A full-parameter unidirectional metamaterial cloak for microwaves. *Nat. Mater.* **12**, 25–28 (2013).
6. Liu, R. et al. Broadband ground-plane cloak. *Science* **323**, 366–369 (2009).
7. Alù, A. & Engheta, N. Achieving transparency with plasmonic and metamaterial coatings. *Phys. Rev. E* **72**, 016623 (2005).
8. Edwards, B., Alù, A., Silveirinha, M. G. & Engheta, N. Experimental verification of plasmonic cloaking at microwave frequencies with metamaterials. *Phys. Rev. Lett.* **103**, 153901 (2009).
9. Yu, N. et al. Light propagation with phase discontinuities: generalized laws of reflection and refraction. *Science* **334**, 333–337 (2011).
10. Ni, X., Wong, Z. J., Mrejen, M., Wang, Y. & Zhang, X. An ultrathin invisibility skin cloak for visible light. *Science* **349**, 1310–1314 (2015).
11. Yang, Y. et al. Full-polarization 3D metasurface cloak with preserved amplitude and phase. *Adv. Mater.* **28**, 6866–6871 (2016).
12. Zigoneanu, L., Popa, B. I. & Cummer, S. A. Three-dimensional broadband omnidirectional acoustic ground cloak. *Nat. Mater.* **13**, 352–355 (2014).
13. Farhat, M., Guenneau, S. & Enoch, S. Ultrabroadband elastic cloaking in thin plates. *Phys. Rev. Lett.* **103**, 024301 (2009).
14. Han, T. et al. Experimental demonstration of a bilayer thermal cloak. *Phys. Rev. Lett.* **112**, 054302 (2014).
15. Ma, W., Cheng, F. & Liu, Y. Deep-learning enabled on-demand design of chiral metamaterials. *ACS Nano* **12**, 6326–6334 (2018).
16. Malkiel, I. et al. Plasmonic nanostructure design and characterization via deep learning. *Light Sci. Appl.* **7**, 60 (2018).
17. Raccuglia, P. et al. Machine-learning-assisted materials discovery using failed experiments. *Nature* **533**, 73–76 (2016).
18. Peurifoy, J. et al. Nanophotonic particle simulation and inverse design using artificial neural networks. *Sci. Adv.* **4**, eaar4206 (2018).
19. Li, H. et al. Dual-band Fresnel zone plate antenna with independently steerable beams. *IEEE Trans. Antennas Propag.* **66**, 2113–2118 (2018).
20. Cui, T. J., Qi, M. Q., Wan, X., Zhao, J. & Cheng, Q. Coding metamaterials, digital metamaterials and programmable metamaterials. *Light Sci. Appl.* **3**, e218 (2014).

21. Xu, C., Stiubianu, G. T. & Gorodetsky, A. A. Adaptive infrared-reflecting systems inspired by cephalopods. *Science* **359**, 1495–1500 (2018).
22. Taflove, A. & Hagness, S. C. *Computational Electrodynamics: The Finite-Difference Time-Domain Method* (Artech House, 2000).
23. Qian, C. et al. Transient response of a signal through a dispersive invisibility cloak. *Opt. Lett.* **41**, 4911–4914 (2016).
24. Zheludev, N. I. & Kivshar, Y. S. From metamaterials to metadevices. *Nat. Mater.* **11**, 917–924 (2012).
25. Shaltout, A. M., Shalaev, V. M. & Brongersma, M. L. Spatiotemporal light control with active metasurfaces. *Science* **364**, eaat3100 (2019).
26. Kwon, H., Sounas, D., Cordaro, A., Polman, A. & Alu, A. Nonlocal metasurfaces for optical signal processing. *Phys. Rev. Lett.* **121**, 173004 (2018).
27. Schmidhuber, J. Deep learning in neural networks: an overview. *Neural Netw.* **61**, 85–117 (2015).
28. Hinton, G. et al. Deep neural networks for acoustic modeling in speech recognition: the shared views of four research groups. *IEEE Signal Process. Mag.* **29**, 82–97 (2012).
29. Ramprasad, R., Batra, R., Pilania, G., Mannodi-Kanakkithodi, A. & Kim, C. Machine learning in materials informatics: recent applications and prospects. *npj Comput. Mater.* **3**, 54 (2017).
30. Carleo, G. & Troyer, M. Solving the quantum many-body problem with artificial neural networks. *Science* **355**, 602–606 (2017).
31. Ye, D., Chang, K., Ran, L. & Xin, H. Microwave gain medium with negative refractive index. *Nat. Commun.* **5**, 5841 (2014).
32. Constantine, A. B. *Antenna Theory: Analysis and Design* (Wiley, 2005).
33. Zhang, Y. & Ng, B. P. MUSIC-like DOA estimation without estimating the number of sources. *IEEE Trans. Signal Process.* **58**, 1668–1676 (2010).
34. Qian, C. et al. Experimental observation of superscattering. *Phys. Rev. Lett.* **122**, 063901 (2019).
35. Selvanayagam, M. & Eleftheriades, G. V. Experimental demonstration of active electromagnetic cloaking. *Phys. Rev. X* **3**, 041011 (2013).
36. Park, J., Kang, J., Kim, S., Liu, X. & Brongersma, M. Dynamic reflection phase and polarization control in metasurfaces. *Nano Lett.* **17**, 407–413 (2017).
37. Wang, Q. et al. Optically reconfigurable metasurfaces and photonic devices based on phase change materials. *Nat. Photon.* **10**, 60–65 (2016).
38. Tian, Z. et al. Reconfigurable vanadium dioxide nanomembranes and microtubes with controllable phase transition temperatures. *Nano Lett.* **18**, 3017–3023 (2018).
39. Ma, X. et al. An active metamaterial for polarization manipulating. *Adv. Opt. Mater.* **2**, 945–949 (2014).
40. Sarabandi, K. & Behdad, N. A frequency selective surface with miniaturized elements. *IEEE Trans. Antennas Propag.* **55**, 1239–1245 (2007).
41. Widrow, B., Mantey, P. E., Griffiths, L. J. & Goode, B. B. Adaptive antenna systems. *Proc. IEEE* **55**, 2143–2159 (1967).
42. Aeschlimann, M. et al. Adaptive subwavelength control of nano-optical fields. *Nature* **446**, 301–304 (2007).
43. Colton, D. & Kress, R. *Inverse Acoustic and Electromagnetic Scattering Theory* (Springer, 1997).
44. Rodriguez-Nieva, J. F. & Scheurer, M. S. Identifying topological order through unsupervised machine learning. *Nat. Phys.* **15**, 790–795 (2019).
45. Hughes, T. W., Minkov, M., Shi, Y. & Fan, S. Training of photonic neural networks through in situ backpropagation and gradient measurement. *Optica* **5**, 864–871 (2018).
46. Lin, X. et al. All-optical machine learning using diffractive deep neural networks. *Science* **361**, 1004–1008 (2018).

Methods

Characterization of the meta-atom, data generation and ANN training. An SMV2019-079LF commercial varactor diode was used and modelled by the commercial software Advanced Design System to extract the effective RLC parameters (Supplementary Notes 1 and 2). The numerical simulation package CST Microwave Studio was employed to generate the reflection response database via Monte Carlo sampling, as a function of bias voltage, incident angle and frequency. The reflection spectrum measurement of the fabricated flat metasurface is described in Supplementary Note 4. After obtaining the data, the ANN was trained for the mapping {incident wave and reflection spectrum} → {bias voltage} for individual meta-atoms, implemented using Python version 3.5.0. and TensorFlow framework version 1.10.0 (Google) on a server (GeForce GTX TITAN X GPU and Intel(R) Xeon(R) CPU X5570 at 2.93 GHz with 48 GB RAM, running a Linux operating system; Supplementary Note 8).

FDTD simulations. The simulation set-up is described in Supplementary Note 3. The frequency of the incident wave was extracted by Fourier-transforming the received continuous signal, and the incident angle was calculated by comparing the phases of the received signal obtained from different spatial points. The surrounding background was known hypothetically, but in the experiment it was detected in real time.

Experimental self-adaptive cloak system. For detection of the incident wave (frequency and incident angle), we attached an ultra-wideband Vivaldi antenna (gain of 7 dBi and a working band of 1.4–10.5 GHz) onto a plastic disc connected to a stepper motor (Supplementary Note 5). The stepper motor had a no-load speed of 2,000 r.p.m. at 24 V. To avoid scattered waves from the background or cloak, which would unfavourably affect detection of the incident wave from the top, we placed the detector on an absorber beside the cloak. The surrounding landform was detected by an Intel RealSense D435i depth camera at 90 frames per second (Supplementary Note 5). The detected information was fed into the pretrained ANN, and all required voltages were instantly supplied by digital-to-analog converters and voltage amplifiers connected to the Linux OS on an ARM board. We measured the near-field magnetic field and far-field RCS to check the performance of the intelligent cloak (see Supplementary Note 6 for measurement details).

Data availability

The data that support the plots within this paper and other findings of the study are available from the corresponding author upon reasonable request.

Code availability

The custom codes used in this study are available from the corresponding author upon reasonable request.

Acknowledgements

We thank P. Rebusco and I. Kaminer for critical reading and editing of the manuscript, L.W. Tian for assistance with experimental construction, and J. T. Huangfu, D. S. Liao and Y. Z. Ding for discussions. This work was sponsored by the National Natural Science Foundation of China under grants 61625502, 11961141010, 61574127 and 61975176, the Top-Notch Young Talents Program of China and the Innovation Joint Research Center for Cyber-Physical-Society System. B.Z. was supported by the National Natural Science Foundation of China under grant 61601408. L.S. was supported by the National Natural Science Foundation of China under grant 61905216. C.Q. was supported by the Chinese Scholarship Council (CSC number 201906320294) and a Zhejiang University Academic Award for Outstanding Doctoral Candidates.

Author contributions

C.Q. and H.C. conceived the idea. C.Q. performed the numerical simulations and the experiment. C.Q. and H.C. wrote the manuscript. B.Z., Y.S., L.J., E.L. and L.S. discussed the results and commented on the manuscript. H.C. supervised the project.

Competing interests

The authors declare no competing interests.

Additional information

Supplementary information is available for this paper at https://doi.org/10.1038/s41566-020-0604-2.

Correspondence and requests for materials should be addressed to H.C.

Reprints and permissions information is available at www.nature.com/reprints.